New Journal of Physics
The open access journal at the forefront of physics

Deutsche Physikalische Gesellschaft DPG
IOP Institute of Physics

Published in partnership with: Deutsche Physikalische Gesellschaft and the Institute of Physics

OPEN ACCESS

RECEIVED
12 July 2015

REVISED
30 November 2015

ACCEPTED FOR PUBLICATION
16 December 2015

PUBLISHED
4 January 2016

PAPER

Optimal control of laser-induced spin–orbit mediated ultrafast demagnetization

P Elliott[1], **K Krieger**[1], **J K Dewhurst**[1], **S Sharma**[1,2] **and E K U Gross**[1]

[1] Max-Planck-Institut für Mikrostrukturphysik, Weinberg 2, D-06120 Halle, Germany
[2] Department of physics, Indian Institute for technology-Roorkee, 247667 Uttarkhand, India

E-mail: pelliott@mpi-halle.mpg.de

Keywords: TDDFT, QOCT, laser induced spin dynamics, demagnetization, coherent control

Abstract

Laser induced ultrafast demagnetization is the process whereby the magnetic moment of a ferromagnetic material is seen to drop significantly on a timescale of 10–100 s of femtoseconds due to the application of a strong laser pulse. If this phenomenon can be harnessed for future technology, it offers the possibility for devices operating at speeds several orders of magnitude faster than at present. A key component to successful transfer of such a process to technology is the controllability of the process, i.e. that it can be tuned in order to overcome the practical and physical limitations imposed on the system. In this paper, we demonstrate that the spin–orbit mediated form of ultrafast demagnetization recently investigated (Krieger *et al* 2015 *J. Chem. Theory Comput.* **11** 4870) by *ab initio* time-dependent density functional theory (TDDFT) can be controlled. To do so we use quantum optimal control theory (OCT) to couple our TDDFT simulations to the optimization machinery of OCT. We show that a laser pulse can be found which maximizes the loss of moment within a given time interval while subject to several practical and physical constraints. Furthermore we also include a constraint on the fluence of the laser pulses and find the optimal pulse that combines significant demagnetization with a desire for less powerful pulses. These calculations demonstrate optimal control is possible for spin–orbit mediated ultrafast demagnetization and lays the foundation for future optimizations/simulations which can incorporate even more constraints.

Introduction

Faster, smaller, and more efficient future technology could be achieved if we could master control over the charge and spin dynamics of electrons on the nanoscale [1]. However precisely at these very short length and time scales, quantum effects are strong, which makes it difficult to exert this control. A long standing goal of modern physics is to address this problem using tailored laser pulse [2–10]. With the advent [11] of laser pulse shapers that can tailor the laser field to a given shape, there was now a tool that could be used for control of quantum dynamics. The challenge is finding the shape of the laser pulse that produces the desired dynamics.

Optimal control theory (OCT) is a method developed [12, 13] in both Mathematics and Engineering to solve the problem of finding a particular control variable that gives a desired outcome. In general OCT works by creating a target functional of the control field calculated from simulation of the system. Then any constraints on the system are incorporated using penalty functionals, before extremizing the total functional to find the optimal field. OCT can be extended to the realm of quantum mechanics by constructing the target functional using observables given by the time-dependent schrödinger equation (TDSE).

The electron dynamics given by propagating the TDSE is, for more than a handful of electrons, a computationally intractable problem due to the coulomb interaction between electrons and an alternative approach must be used. Time-dependent density functional theory (TDDFT) is one such approach, which works by mapping the problem to a non-interacting system [14], referred to as the Kohn–Sham (KS) system. This system is defined such that propagating electrons in this system will reproduce the same time dependent

density (the probability to find an electron at any given point) as propagating in the exact system using the TDSE. As the KS system is non-interacting, the problem is now computationally tractable, and has been successful in predicting absorption spectra of a large range of atoms, molecules, and solids [15–17]. Thus TDDFT is an outstanding candidate to couple to OCT [18] for control of quantum dynamics, and has been used successfully for control of charge transfer [19], HHG [22], strong-field ionization [20, 21], bond-breaking [23], among others.

Laser-induced ultrafast demagnetization was first observed in the mid 1990s, whereby a strong femtosecond laser pulse caused a significant loss of the magnetic moment of a thin film of Ni in a time less than 1ps [24]. Since then, this phenomena has been the subject of much experimental [25–35] and theoretical [36–40] endeavor and several mechanisms have been proposed to explain the demagnetization. In [40], *ab initio* TDDFT simulations were performed to investigate the demagnetization and found that when spin–orbit interaction was included in the system Hamiltonian, a loss of moment was observed for very short (5 fs), very intense (1×10^{15} W cm^{-2}) laser pulses. It is this system we wish to control by varying the intensity and frequency of the laser pulse, subject to several practical constraints, in order to maximize the total loss of moment. To do so we utilize the framework developed in [18, 23, 41] which combines OCT with quantum simulations of spin dynamics.

Background and methods

We begin by briefly reviewing TDDFT and OCT, a more thorough discussion can be found here [18].

TDDFT

The electronic density is defined as

$$n(\mathbf{r}, t) = N \int \mathrm{d}\mathbf{r}_2 \ldots \mathrm{d}\mathbf{r}_N \, \Psi^*(\mathbf{r}, \mathbf{r}_2, \ldots, \mathbf{r}_N, t) \times \Psi(\mathbf{r}, \mathbf{r}_2, \ldots, \mathbf{r}_N, t), \tag{1}$$

where N is the total number of electrons, $\mathbf{r}$ is the spacial coordinate, t is the time, and Ψ is the wavefunction of the TDSE:

$$\mathrm{i}\frac{\partial}{\partial t}\Psi = \hat{H}\Psi \tag{2}$$

for Hamiltonian:

$$\hat{H} = \hat{T} + \hat{V}_{\mathrm{ext}} + \hat{V}_{\mathrm{ee}} \tag{3}$$

composed of the kinetic energy, $\hat{T}$, the electron–electron interaction, $\hat{V}_{\mathrm{ee}}$, and the external potential, $\hat{V}_{\mathrm{ext}}$, which includes both the electron-nuclear interaction and the electric fields of any laser pulses. We use atomic units throughout unless otherwise stated. TDDFT is founded upon the Runge–Gross theorem [14] which proves a 1 −1 correspondence between the time-dependent density and the time-dependent external potential (up to a time-dependent constant) for any electron–electron interaction. Hence all observables of the system are, in principle, unique functionals of the density. In particular, a non-interacting KS system [42] can be defined with a unique KS potential that reproduces the time-dependent density of the interacting system and thus predicts all observables of the true system without requiring the costly propagation of equation (2). The TDKS equation is:

$$\mathrm{i}\frac{\partial}{\partial t}\phi_j(\mathbf{r}, t) = \left[-\frac{\nabla}{2} + v_{\mathrm{S}}(\mathbf{r}, t)\right]\phi_j(\mathbf{r}, t) \tag{4}$$

with the total density given by

$$n(\mathbf{r}, t) = \sum_{j=1}^{N} |\phi_j(\mathbf{r}, t)|^2 \tag{5}$$

The KS potential, $v_{\mathrm{S}}(\mathbf{r}, t)$, consists of three pieces:

$$v_{\mathrm{S}}(\mathbf{r}, t) = v_{\mathrm{ext}}(\mathbf{r}, t) + v_{\mathrm{H}}(\mathbf{r}, t) + v_{\mathrm{XC}}(\mathbf{r}, t), \tag{6}$$

where $v_{\mathrm{H}}(\mathbf{r}, t)$ is the usual Hartree potential of the instantaneous density, and $v_{\mathrm{XC}}(\mathbf{r}, t)$ is the exchange correlation (XC) potential and is a functional of the density at all previous times, the interacting initial state, and the non-interacting initial KS state. In practice, it must be approximated, with the most common approximation being the adiabatic local density approximation (ALDA):

$$v_{\mathrm{XC}}[n](\mathbf{r}, t) = v_{\mathrm{XC}}^{\mathrm{LDA}}[n(\mathbf{r}, t)] = \left.\frac{\mathrm{d}e_{\mathrm{XC}}^{\mathrm{unif}}}{\mathrm{d}n}\right|_{n=n(\mathbf{r},t)} \tag{7}$$

which uses just the instantaneous density inputed into the ground-state DFT LDA XC functional and $e_{XC}^{unif}(n)$ is the XC energy density of the uniform electron gas. The initial KS state is typically the ground-state found from a DFT calculation.

From this starting point, TDDFT has been extended to include non-collinear magnetism and magnetic fields [43]. For this case, we have a non-interacting Pauli KS Hamiltonian [44] which is used to propagate two component spinors, from which the density and magnetization density exactly replicate those of the interacting system. This is the formulation we will use for our simulations. The magnetization density operator may be written as:

$$\hat{\mathbf{m}}(\mathbf{r}) = \hat{\mathbf{M}}\,\hat{n}(\mathbf{r}), \tag{8}$$

where $\hat{n}(\mathbf{r})$ is the density operator and in the two-component spinors propagated in our calculations, $\hat{\mathbf{M}} = -g\mu_B\hat{\mathbf{S}}$ and $\mathbf{S} = \boldsymbol{\sigma}/2$ where $\{\sigma_x, \sigma_y, \sigma_z\}$ are the familiar Pauli spin matrices and g is the electronic gyromagnetic ratio ($g = 2$ for our purposes). For periodic boundary conditions, the total moment is then

$$\mathbf{M}(t) = \int_{\Omega} \mathrm{d}^3 r\ \mathbf{m}(\mathbf{r}, t), \tag{9}$$

where Ω is a single unit cell. The KS Hamiltonian for our simulations is:

$$\begin{aligned}\hat{H}_S(t) = \frac{1}{2}\left(\hat{\mathbf{p}} + \frac{1}{c}\mathbf{A}_{ext}(t)\right)^2 + v_S(\hat{\mathbf{r}}, t) \\ + \frac{1}{c}\hat{\mathbf{S}}\cdot\mathbf{B}_S(\hat{\mathbf{r}}, t) + \frac{1}{2c^2}\hat{\mathbf{S}}\cdot(\nabla v_S(\hat{\mathbf{r}}, t)\times\hat{\mathbf{p}}),\end{aligned} \tag{10}$$

where $\hat{\mathbf{p}}$ is the momentum operator, $\hat{\mathbf{S}}$ is the vector spin operator, and c is the speed of light. The laser pulse electric field is written as a vector potential, $\mathbf{A}_{ext}(t)$ in the velocity gauge as it allows Bloch's theorem to be utilized. The KS magnetic field is written as $\mathbf{B}_S(\hat{\mathbf{r}}, t) = \mathbf{B}_{ext}(t) + \mathbf{B}_{XC}(\hat{\mathbf{r}}, t)$, where $\mathbf{B}_{ext}(t)$ is the magnetic field of the applied electromagnetic field and $\mathbf{B}_{XC}(\hat{\mathbf{r}}, t)$ is the XC magnetic field. The ALDA can be extended to $\mathbf{B}_{XC}$ using the LDA rotation method of Kübler [45]. The final term of equation (10) is the spin–orbit coupling (SOC) term, which can be thought of as the interaction between the spin of an electron and the effective magnetic field caused by relativistic motion thought a scalar potential. In a centrosymmetric potential, this term reduces to the well known $\hat{\mathbf{L}}\cdot\hat{\mathbf{S}}$ coupling. Propagation with Hamiltonian equation (10) is implemented in ELK [46], an all-electron electronic structure code, which was also used for all ground state and time-dependent calculations.

Optimal control theory

The central quantity of OCT is the target functional $G[u]$:

$$G[u] = G[\Psi[u], u] = J_1[u] + J_2[u], \tag{11}$$

where u is the control field and $\Psi[u]$ contains the information on how the system responds to the control field. In quantum OCT (QOCT), $\Psi[u]$ is then the wavefunction, which is a functional of the control field via the TDSE and from which any system observables to be controlled may be calculated. The target functional is generally separated into two pieces, $J_1[u]$ which contains information on the desired dynamics and $J_2[u]$ which is a penalty function in order to satisfy any constraints on the system or control field. The magnitude of the penalty functional is determined by how strongly a constraint must be satisfied.

Once a relevant target functional has been constructed, the goal of OCT is to extremize it and thus find the optimal control field u to best satisfy the balance between desired dynamics and the constraints. There are many choices for the algorithm to perform this optimization, some are general, such as the Nelder–Mead [47], NEWOAU [48], or conjugate gradient [49] algorithms, while some are developed for specific types of problem, e.g. in QOCT the ZBR scheme [50] adds a time dependent auxiliary wavefunction, which is also propagated in time and the overlap with the true wavefunction used to construct the control field.

For our system, we wish to maximize the loss of magnetic moment in a given time interval $[0, T]$ while including practical and physical constraints on the type of laser pulse. Thus $\epsilon(t)$, the electric field of the laser pulse is the control field and

$$J_1[\epsilon] = \langle\Psi[\epsilon](T)|\hat{\mathbf{M}}_z|\Psi[\epsilon](T)\rangle = M_z(T) \tag{12}$$

is the target functional to be minimized, i.e. if we choose the initial magnetization $M_z(0)$ of the ferromagnet to be along the z-axis, then minimizing $M_z(T)/M_z(0)$ will maximize the loss of moment.

The constraints on the electric field are that the pulses satisfy Maxwell's equations (details below) and only certain frequencies are used to construct the pulse. The second constraint is of practical nature, as experimentally, pulses containing arbitrary frequencies cannot be constructed and often access to a single frequency (or multiples thereof) is only available. From Maxwell's equations, the following constraints on the electric field must be physically satisfied:

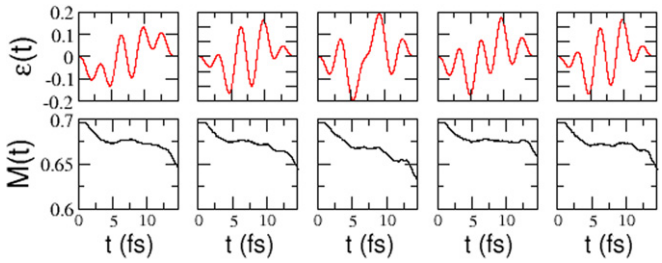

Figure 1. Upper panels: the electric fields for initialization laser pulses. Lower panels: the dynamics of the total moment in the z-direction for each pulse.

$$\int_0^T \mathrm{d}t\epsilon\,(t) = 0, \tag{13}$$

$$\epsilon\,(0) = 0 = \epsilon\,(T). \tag{14}$$

Following [23], we can satisfy all these constraints by writing the electric field

$$\epsilon\,(t) = \sum_{n=1}^{N_\omega} \tilde{\epsilon}_n \sin(\omega_n t)\sin^2(\frac{\pi t}{T}), \tag{15}$$

where N_ω is the number of frequencies to be used and $\tilde{\epsilon}_n$ are the coefficients to be optimized. It can be seen that this choice automatically satisfies the constraints from Maxwell's equations if $\omega_n T$ is a multiple of 2π. A convenient choice for the frequencies is

$$\omega_n = \frac{2\pi n}{T} \tag{16}$$

which will be used in the first of our optimizations. We emphasize that in a realistic control problem these frequencies are dictated by the experimental setup and not by the optimal control formalism. In our demonstration, they where simply chosen for convenience.

Results

In [40] TDDFT simulations for laser-induced demagnetization in bulk Ni were performed. A loss of the total magnetic moment was observed in all cases, and the fraction of moment lost was shown to be dependent on the field intensity and carrier frequency. Hence the system was a strong candidate for optimal control. The purpose of this work is to demonstrate optimal control of the ultrafast demagnetization in bulk Ni by attempting to maximize the loss of moment after $T = 14.5$ fs. The choice of this time is arbitrary and will be determined by the experimental setup. For this work, the value was chosen based upon the fastest timescale for spin–flip demagnetization seen in [40]. As one of the major experimental constraints is in the choice of available frequencies from which to build the laser pulse, we will include this constraint by using an electric field of the form given by equation (15) using $N_\omega = 4$ different laser frequencies, as defined by equation (16). For the optimization we choose to use the gradient-free Nelder–Mead simplex algorithm. To initialize the Nelder–Mead algorithm, $N_\omega + 1$ starting points are required, it is instructive to examine these before moving to the results of the optimization.

Maximize demagnetization

To initialize our calculations[3], we construct five different pulses where the coefficients of equation (15) are chosen at random in a suitable range. These pulses may be seen in the upper panel of figure 1. The dynamics of $M_z(t)$ are shown in the lower panel and it can be seen that all pulses display demagnetization. If we look at the final time, the average loss of moment is approximately 7%. If the optimal control is successful, then this percentage loss should be significantly increased.

From the initial pulses, the Nelder–Mead algorithm then calculates a new set of coefficients from a simple set of rules and then tests how this affects the target functional by performing a TDDFT simulation with the laser field given by these coefficients. It then iterates this procedure and traverses the multidimensional parameter space, searching for the optimal set of coefficients.

[3] All calculations are performed with a time step of 0.1 au and $8 \times 8 \times 8k$-points.

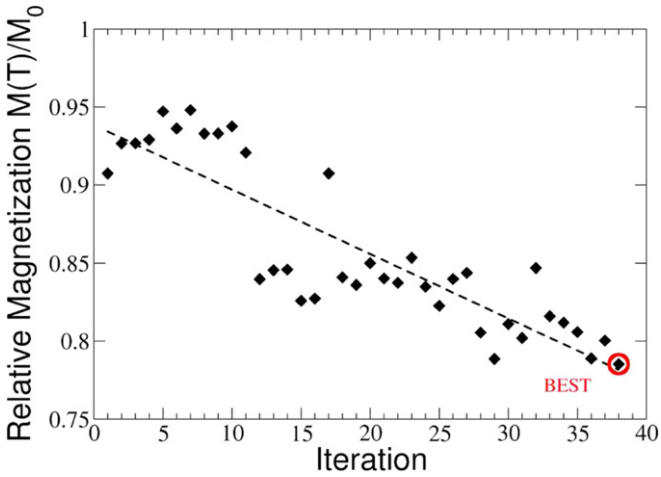

Figure 2. The fraction of magnetic moment loss for each iteration of the Nelder–Mead optimization and the trend in the optimal control.

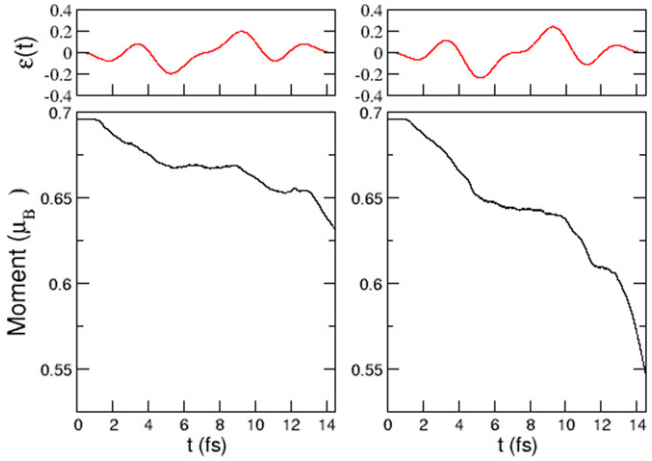

Figure 3. Upper panels: the electric fields[4] for the optimal laser pulse found after 38 iteration of the optimal control algorithm (right) and, for comparison, the 3rd initialization pulse (left). Lower panels: the corresponding dynamics of M_z for these pulses.

In figure 2, we plot the ratio of the final moment after time T to the initial moment for each of the iterations. Although individual iterations can worsen the loss percentage, there is a clear downward trend as better and better pulses are found during the search, indicating that the optimal control is not only applicable to this problem but also is crucial from obtaining higher demagnetization.

Each set of coefficients is a point in the parameter space, at each iteration, the Nelder–Mead algorithm reflects the worst point through the center of mass of the other points. Depending on whether this new point improves upon the next worst point, the algorithm can expand or contract in this direction, otherwise it can reduce all points towards the best point. This explains why individual points may worsen the ratio $M_z(T)/M_z(0)$.

If we look at the result after 38 iterations, the best pulse the optimal control procedure has found causes a 20% loss of moment. This is at least twice as much as the random initial pulses used to start the algorithm and is a clear demonstration that the moment can be successfully controlled using OCT. In figure 3 we show the electric field of this best pulse and also the magnetization dynamics, compared to an initial pulse. Examining the pulse shape compared to the initial pulses of figure 1, there is no obvious reason why one leads to a larger demagnetization. This is the power of QOCT to find such pulses. In [40], it was found that the demagnetization process has a highly nonlinear dependence on the pulse intensity of fluence. The optimal pulse shown in figure 3 has a significantly higher fluence compared to the initial pulse which combined with the nonlinearity of the problem leads to a larger loss of the magnetic moment. It was also found in [40] that demagnetization can occur for a period after the laser pulse. In this case we can see in figure 3 that if we simulate for a longer time, we will

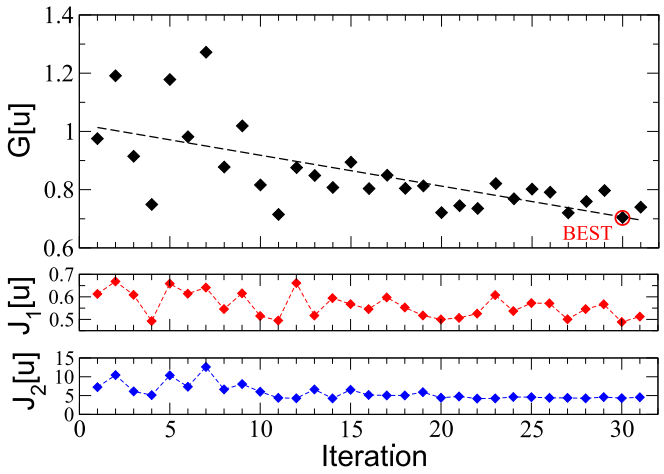

Figure 4. The OCT target functional, $G[u] = J_1[u] + 0.05 \times J_2[u]$, where $J_1[u] = M_z[u](T)/M_z(0)$ and $J_2[u] = \int_0^T \mathrm{d}t\ u^2(t)$, for the electric field $u = \epsilon(t)$ at each iteration of the algorithm.

likely see further demagnetization with our pulses. However, the optimal control algorithm has no knowledge of this and simply maximizes the loss of moment at time T, regardless of what might happen after. It suggests for future optimizations, a better target functional might be to look at a time slightly later than when the pulse finishes or to average the moment during a period after the pulse.

Fluence constraint

For practical reasons, the fluence of the applied pulse should be constrained. The primary reason is simply efficiency—achieving the same dynamics as a higher energy pulse but using a lower energy pulse. Other reasons include surface damage to the material due to high fluence pulses, heating of the sample (and problems associated with cooling it), or physical restrictions on the laser itself preventing production of high fluence pulses. All of these present significant problems to future technological application, hence we include a fluence constraint into our calculations.

If we add to equation (11), the constraint

$$J_2[\epsilon] = \alpha \int_0^T \mathrm{d}t\ \epsilon^2(t) \tag{17}$$

which is proportional to the laser fluence. The free parameter α determines how strong the constraint is, for this calculation we choose $\alpha = 0.05$. This parameter was based on examining the results of the previous optimization and choosing α to favor a lower fluence while still maintaining significant demagnetization in the set. In this example we choose a time period of $T = 16.21$ fs and frequencies of $\omega_1 = 0.075$ au, $\omega_2 = \frac{9}{8}\omega_0$, $\omega_3 = \frac{10}{8}\omega_0$ and $\omega_4 = \frac{11}{8}\omega_0$. These also satisfy the constraints of equations (13) and (14) and approximately span the optical frequency range.

In figure 4, we show the value of the total target functional, equation (11), for each iteration of the optimization algorithm. Unlike the previous case, we cannot attach a physical meaning to the target functional, so the actual value is not significant, only the trend. Furthermore, when choosing α, it was clear that the parameter space is a more complicated environment than the previous case, as a pulse could have the same value of equation (11) by either increasing the demagnetization or decreasing the fluence. We again initialize the search using random coefficients. As the optimization is computationally expensive[5], we stopped the optimization after 26 iterations, although this was sufficient to see the trend and demonstrate optimal control.

To see the power of this optimization, in figure 5 we plot the electric fields and the dynamics of $M_z(t)$ for two different pulses. These correspond to the best point of figure 4 and a reference pulse corresponding to the $G = 1.191$ point. This point was chosen to demonstrate the need for optimal control as the total fluence is significantly more (8872 mJ cm^{-2}) than the best point found (3665 mJ cm^{-2}), yet yielded a worse final moment (33% loss compared to 50%). Thus we can use OCT to find better pulses that cost far less in terms of energy. Even comparing to the best random initial guess, the algorithm was able to reduce the fluence by 15% while

[4] The initial pulse has a fluence of 4023 mJ cm^{-2} while the optimized pulse has a fluence of 5702 mJ cm^{-2}.

[5] Each iteration required 5000 CPU hours.

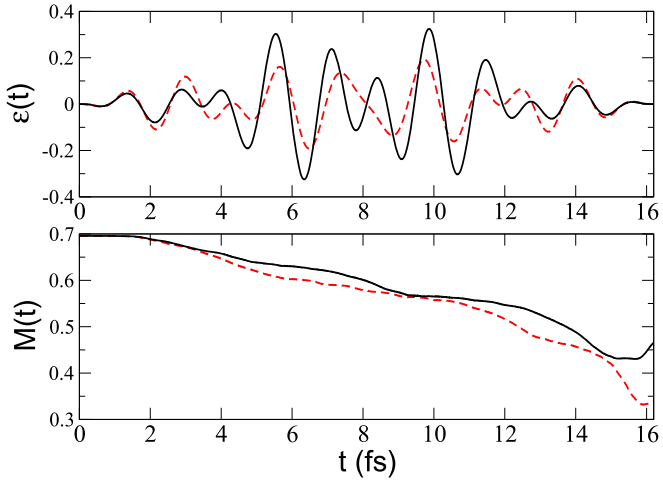

Figure 5. The electric field $\epsilon\ (t)$ (upper panel) and total magnetic moment M_z (lower panel) for the reference pulse (solid black line) and the best pulse (dashed red) found during the fluence constraint optimization.

achieving the same amount of demagnetization. As was detailed in reference [40], the fluence required to see demagnetization of this type may be decreased by several orders of magnitude when longer duration pulses are used. So while the fluences in this demonstration are quite large, we are confident the results will be similar if applied to longer duration pulses. Furthermore, in subsequent work [51] to [40], we have simulated a pulse based on experimental parameters (intensity of 3.8 $\times$ 1011 W cm^{-2}, fluence 8.05 mJ cm^{-2}, and a FWHM of 40 fs) and still see a 20% loss in moment due to spin–orbit effects. The underlying physics in this case is the same as for the short pulses. Thus we anticipate that the controllability found in this work will also be true for lower energy laser pulses.

Conclusions

In summary we have achieved the optimal control of spin–orbit mediated ultrafast demagnetization. We showed that the loss of moment can be at least doubled (compared to randomly chosen typical pulses) for a system where the available laser frequencies (used to tailor the laser pulse) are constrained. Furthermore, we extended the control problem to include a constraint on the laser fluence and demonstrated that QOCT could successfully find a pulse that balances the fluence and demagnetization requirements. Compared to a reference pulse, this optimal pulse produces more favorable magnetization dynamics, while reducing the fluence by over a factor of 2. Control of the system is of upmost importance for future technological application (for example, in spintronics), where the desired dynamics and constraints are dictated by practical concerns. Any physical phenomenon must be robust to these concerns, and as we have demonstrated, this form of ultrafast demagnetization meets this criteria. Simulation and QOCT of more complicated scenarios, such as longer pulse durations or further constraints on the fluence, intensity, and robustness of the demagnetization, can be build upon this foundation.

Acknowledgments

This work is supported by SFB 762 of the Deutsche Forschungsgemeinschaft.

References

[1] Kirilyuk A, Kimel A V and Rasing T 2010 Ultrafast optical manipulation of magnetic order *Rev. Mod. Phys.* **82** 2731
[2] Peirce A P, Dahleh M A and Rabitz H 1988 Optimal control of quantum-mechanical systems: existence, numerical approximation and applications *Phys. Rev.* A **37** 4950
[3] Kosloff R, Rice S A, Gaspard P, Tersigni S and Tannor D J 1989 Wavepacket dancing: achieving chemical selectivity by shaping light pulses *Chem. Phys.* **139** 201
[4] Huang G M, Tarn T J and Clark J W 1983 On the controllability of quantum-mechanical systems *J. Math. Phys.* **24** 2608
[5] Rabitz H, de Vivie-Riedle R, Motzkus M and Kompa K 2000 Whither the future of controlling quantum phenomena? *Science* **288** 824
[6] Corkum P B and Krausz F 2007 Attosecond science *Nat. Phys.* **3** 381
[7] Cong S 2014 *Control of Quantum Systems: Theory and Methods* (Singapore: Wiley)
[8] Xi N, Zhang M and Li G 2013 *Modeling and Control for Micro/Nano Devices and Systems* (Boca Raton, FL: CRC Press)

[9] Reich D, Ndong M and Koch Christiane P 2012 Monotonically convergent optimization in quantum control using Krotovs method *J. Chem. Phys.* **136** 104103
[10] Levin L, Skomorowski W, Rybak L, Kosloff R, Koch C P and Amitay Z 2015 Coherent control of bond making *Phys. Rev. Lett.* **114** 233003
[11] Weiner A M, Leaird D E, Patel J S and Wullert J R 1992 Programmable shaping of femtosecond pulses by use of a 128-element liquid–crystal phase modulator *IEEE J. Quantum Electron* **28** 908
[12] Bryson A E and Ho Y-C 1975 *Applied Optimal Control* (Washington, DC: Hemisphere)
[13] Luenberger D G 1979 Introduction to Dynamic Systems: Theory *Models, and Applications* (New York: Wiley)
[14] Runge E and Gross E K U 1984 Density-functional theory for time-dependent systems *Phys. Rev. Lett.* **52** 997
[15] Elliott P, Furche F and Burke K 2009 Excited states from time-dependent density functional theory *Reviews in Computational Chemistry* ed K B Lipkowitz and T R Cundari (Hoboken, NJ: Wiley) pp 91–165
[16] Marques M A L, Maitra N T, Nogueira F, Gross E K U and Rubio A (ed) 2012 *Fundamentals of Time-Dependent Density Functional Theory* (*Lecture Notes in Physics* vol 837) (Berlin: Springer)
[17] Ullrich C A 2011 *Time-Dependent Density-Functional Theory Concepts and Applications* (Oxford: Oxford University Press)
[18] Werschnik J and Gross E K U 2007 Quantum optimal control theory *J. Phys. B: At. Mol. Opt. Phys* **40** R175
[19] Räsänen E, Castro A, Werschnik J, Rubio A and Gross E K U 2008 Optimal laser-control of double quantum dots *Phys. Rev.* B **77** 085324
[20] Hellgren M, Räsänen E and Gross E K U 2013 Optimal control of strong-field ionization with time-dependent density-functional theory *Phys. Rev.* A **88** 013414
[21] Shvetsov-Shilovski N I, Madsen L and Räsänen E 2015 Suppression of strong-field ionization by optimal pulse shaping: application to hydrogen and hydrogen molecular ion *Phys. Rev.* A **91** 023425
[22] Solanpää J, Budagosky J A, Shvetsov-Shilovski N I, Castro A, Rubio A and Räsänen E 2014 Optimal control of high-harmonic generation by intense few-cycle pulses *Phys. Rev.* A **90** 053402
[23] Krieger K, Castro A and Gross E K U 2011 Optimization schemes for selective molecular cleavage with tailored ultrashort laser pulses *Chem. Phys.* **391** 50
[24] Beaurepaire E, Merle J-C, Daunois A and Bigot J-Y 1996 Ultrafast spin dynamics in ferromagnetic nickel *Phys. Rev. Lett.* **76** 4250
[25] Agranat M B, Ashitkov S I, Granovskii A B and Rukman G I 1984 *Sov. Phys. JEPT* **59** 804
[26] Vaterlaus A, Beutler T, Guarisco D, Lutz M and Meier F 1992 *Phys. Rev.* B **46** 5280
[27] Hohlfeld J, Matthias E, Knorren R and Bennemann K H 1997 *Phys. Rev. Lett.* **78** 4861
[28] Scholl A, Baumgarten L, Jacquemin R and Eberhardt W 1997 *Phys. Rev. Lett.* **79** 5146
[29] Aeschlimann M, Bauer M, Pawlik S, Weber W, Burgermeister R, Oberli D and Siegmann H C 1997 *Phys. Rev. Lett.* **79** 5158
[30] Hohlfeld J, Gudde J, Duhr U C O, Korn G and Matthias E 1999 *Appl. Phys.* B **68** 505
[31] Regensburger H, Vollmer R and Kirschner J 2000 *Phys. Rev.* B **61** 14716
[32] Guidoni L, Beaurepaire E and Bigot J Y 2002 *Phys. Rev. Lett.* **89** 017401
[33] Schmidt A B, Pickel M, Wiemhofer M, Donath M and Weinelt M 2005 *Phys. Rev. Lett.* **95** 107402
[34] Melnikov A, Razdolski I, Wehling T O, Papaioannou T E, Roddatis V, Fumagalli P, Aktsipetrov O, Lichtenstein A I and Bovensiepen U 2011 *Phys. Rev. Lett.* **107** 076601
[35] Sultan M, Atxitia U, Melnikov A, Chubykalo-Fesenko O and Bovensiepen U 2012 *Phys. Rev.* B **85** 184407
[36] Hübner W and Bennemann K H 1996 Simple theory for spin-lattice relaxation in metallic rare-earth ferromagnets *Phys. Rev.* B **53** 3422
[37] Zhang G P, Hübner W, Lefkidis G, Bai Y and George T F 2009 *Nat. Phys.* **5** 499
[38] Carva K, Battiato M and Oppeneer P M 2011 *Nat. Phys.* **7** 665
[39] Illg C, Haag M and Fahnle M 2013 Ultrafast demagnetization after laser irradiation in transition metals: *ab initio* calculations of the spin–flip electron–phonon scattering with reduced exchange splitting *Phys. Rev.* B **88** 214404 and references therein.
[40] Krieger K, Dewhurst J K, Elliott P, Sharma S and Gross E K U 2015 Laser-Induced Demagnetization at Ultrashort Time Scales: Predictions of TDDFT *J. Chem. Theory Comput.* **11** 4870
[41] Castro A, Budagosky J and Räsänen E 2015 Private communication within the CRONOS FP7 European project
[42] Kohn W and Sham L J 1965 Self-consistent equations including exchange and correlation effects *Phys. Rev.* A **140** 1133
[43] Capelle K, Vignale G and Györffy B L 2001 Spin currents and spin dynamics in time-dependent density-functional theory *Phys. Rev. Lett.* **87** 206403
[44] von Barth U and Hedin L 1972 A local exchange-correlation potential for the spin polarized case *J. Phys. C: Solid State Phys.* **5** 1629
[45] Kubler J, Hock K-H, Sticht J and Williams A R 1988 Density functional theory of non-collinear magnetism *J. Phys. F: Met. Phys.* **18** 469
[46] elk.sourceforge.net
[47] Nelder J A and Mead R 1965 A simplex method for function minimization *Comput. J.* **7** 308
[48] Powell M J D 2004 *Large Scale Nonlinear Optimization* (New York: Springer) pp 255–297
[49] Hestenes M and Stiefel E 1952 Methods of conjugate gradients for solving linear systems *J. Res. Natl. Bur. Stand.* **49** 409
[50] Zhu W, Botina J and Rabitz H 1998 Rapidly convergent iteration methods for quantum optimal control of population *J. Chem. Phys.* **108** 1953
[51] Krieger K, Elliott P, Dewhurst J K, Sharma S and Gross E K U in preparation